UCRL- 90671
PREPRINT

Dynamical Atom/Surface Effects: Quantum Mechanical Scattering and Desorption

C. Cerjan
R. Kosloff

This paper was prepared for submittal to
Journal of Chemical Physics

April 5, 1984

Dynamical Atom/Surface Effects:

Quantum Mechanical Scattering and Desorption

R. Kosloff

The Dept. of Physical Chemistry

Hebrew University

Jerusalem 91904

Israel

and

C. Cerjan

Lawrence Livermore National Laboratory

Livermore, CA 94550

ABSTRACT

Desorption and scattering of a Helium atom from dynamic surfaces are studied using a Generalized Langevin Equation formalism for the bulk solid and time dependent quantum mechanical propagation of the Helium. The motion of the bulk solid enters the Schrodinger equation as a time dependent potential coupling the solid surface to the atom. The propagation of the atomic wavepacket is then followed in coordinate space using a Fourier transform technique to evaluate the kinetic energy operator. An attenuating grid is used to remove the wavepacket in the asymptotic region thus permitting stable calculations for long duration times. Rates for one dimensional desorption from Tungsten as a function of temperature are computed which display a change in mechanism. Three dimensional scattering from Platinum at two temperatures shows significant non-specular amplitude. These results indicate the utility of this time dependent technique.

I. Introduction

Atom-surface scattering has emerged as a powerful tool in the investigation of solid surface properties.[1] This type of scattering event is eminently suited to surface characterization since the particles do not penetrate the lower layers of the solid and hence do not undergo multiple reflections. Also, the sensitivity of the atomic probe to valence, rather than core, electrons encourages the belief that the observed experimental features will be easily interpretable and provide an accurate representation of the important surface features. New experimental beam techniques are able to provide well-resolved spectra for both elastic and inelastic atom-surface encounters.[2] Sticking probabilities and desorption rates which are important inelastic events are being measured.[3] These advances in the experimental work present a challenge to theoretical methods, since calculations are necessary to identify the important spectral features. Accurate simulation of the experimental results must include elastic and inelastic dynamical quantum mechanical effects. The purpose of this paper is to describe such a dynamical simulation based upon a time-dependent quantum mechanical formalism which incorporates surface motion.

Previous exact quantum mechanical results have concentrated upon close-coupled methods.[4] These techniques can be quite accurate and sensitive for the determination of diffraction peaks and resonances which provide much insight into the nature of the static surface potential.[5] However, the close-coupled formalism has two major disadvantages.

First, the computational effort grows as N^3 where N is the number of channels included. Large unit cells and low incident energies require many channels, and the cost will become prohibitive in these cases. Second, and more importantly, close-coupled methods are based upon a time-independent representation. Manifestly time dependent phenomena, such as surface motions, cannot be treated

For these reasons, classical and semi-classical treatments of atom-surface encounters are the most widely applied methods in simulations of experimental work.[6] In particular, the introduction of the Generalized Langevin formalism[7-12] for the description of thermal motion has extended the applicability of classical trajectory methods to dynamical atom-surface encounters. This classical description of the solid surface is sufficiently accurate for the simulations needed for experimental interpretation. A classical description of the scattering particle, however, is generally inadequate In the following, a consistent scheme is presented which utilizes a classical description of the surface motion and time dependent quantum mechanical propagation for the scattering particle.

Although the time dependent representation in quantum mechanics provides a natural description of the experimental set-up -- preparation of a wave-packet versus a standing wave picture -- and an immediate interpretation in terms of classical trajectory studies, development of time dependent methods has lagged behind other techniques for particle scattering. Early work concentrated upon gas phase reactions[13]; the first application to surface collisions is contained in the work of

Agrawal and Raff.[14] This calculation studied two-dimensional scattering from a dynamical surface using a finite differences algorithm. The surface was constructed as an assembly of harmonic oscillators with the surface temperature introduced by the specification of the initial conditions for these oscillators. The surface-atom interaction was strictly one-sided in the sense that the quantum motion was influenced by the classical dynamics but not conversely. As a result, the total energy was not conserved, and the surface could not absorb energy from the colliding particle.

In addition to these physical limitations, the finite differencing scheme would be extremely difficult to extend to a dynamical three dimensional simulation. An unnecessarily large mesh results from the box boundary conditions, which are not fitted to the infinitely extended surface for the parallel motion and to the free propagating conditions in the normal direction. More importantly, a major difficulty arises from the inaccurate description of the kinetic energy operator. In order to eliminate numerical dispersion[15-16] at least 10 grid points per wave are needed. Computer storage limitations thus present an obstacle to any extension to three dimensions.

It should be mentioned that an approximate three-dimensional calculation for a static surface has been performed for He scattering from LiF.[17] This calculation employs a semi-classical time dependent propagation of Gaussian wavepackets and could, in principle, be extended to dynamical surfaces.

To surmount these difficulties, Fourier transform techniques have been introduced for the integration of the time dependent Schrödinger equation.[15-16] Two dimensional calculations of surface scattering compare favorably with close-coupled results.[18] Likewise, these techniques applied to scattering from a stepped surface have demonstrated the ability of the method to obtain diffraction peaks as well as a direct calculation of resonance lifetimes and sticking probabilities.[19] The Fourier transform is thus a natural choice for dynamical simulations.

II Methodology

A. Physical Background

The simulation of a dynamical encounter between a light He atom and heavy surface atoms is an involved process A complete description requires the solution of a combined many body problem, since the He atom has a relatively large de Broglie wavelength which interacts with several surface atoms simultaneously. In turn, the surface atoms are coupled to the bulk of the crystal atoms which acts as a heat bath. A simulation of the combined dynamics is impossible without a reduction scheme which renders the dynamics into a tractable form

The first step is to write the Hamiltonian of the combined system in a form suitable for reduction

$$H = H_{He} + H_{surf} + H_{bulk} + V_{He-surf} + V_{He-bulk} + V_{surf-bulk} \qquad (2.1)$$

where H_{He} is the free Hamiltonian of He; H_{surf} is the surface atom Hamiltonian; H_{bulk} is the bulk Hamiltonian; $V_{He-surf}$ is the potential

between the surface atoms and the He atom; $V_{He\text{-}bulk}$ is the potential interaction of the bulk atoms with He; and $V_{surf\text{-}bulk}$ is the surface-bulk interaction. The partition of the Hamiltonian used in Equation (2.1) already suggests different ways of treating the He atom, the surface atoms, and the bulk atoms. Because of the wave-like nature of the He atom, it deserves a full quantum mechanical treatment whereas a classical dynamical treatment suffices for the metal surface atoms (except at low surface temperatures). The problem then entails the propagation of a quantum wavepacket which is coupled to the classical surface motion. A great simplification ensues if the translational invariance of the surface is used. By invoking periodic boundary conditions one can restrict the quantum calculation to a finite volume and the classical motion to four surface atoms. For this reduced motion a time dependent quantum mechanical calculation may be coupled to the classical dynamics of the four atoms.

In this mode of representation for the He atom, the time dependent Schrödinger equation was used to propagate the wavefunction. In atomic units

$$i \frac{\partial \Psi}{\partial t} (\underline{R}) = - \frac{\nabla^2}{2m} + V(\underline{R},\underline{r}) + V_o(\underline{R}) \Psi(\underline{R}) \qquad (2.2)$$

where $\underline{R}$ represents the He co-ordinates; $\underline{r} = (\underline{q}_1, \underline{q}_2, \underline{q}_3, \underline{q}_4)$ represents the surface co-ordinates of the unit cell atoms; $V(\underline{R},\underline{r})$ is the surface-He interaction; $V_o(\underline{R})$ is the static He-bulk interaction and m is the He atom mass. The He-surface potential depends parametrically upon the surface co-ordinates hence is a function of time.

Simultaneously the surface atom motion is propagated by using the classical Hamiltonian equation

$$\dot{\underline{p}}_i = - \frac{\partial V}{\partial \underline{q}_i}\,\text{surf} - \left\langle \frac{\partial V}{\partial \underline{q}_i}\,(\underline{R},\underline{r}_i) \right\rangle - \frac{\partial V}{\partial \underline{q}_i}\,\text{surf-bulk} \qquad (2.3)$$

$$\dot{\underline{q}}_i = \underline{p}_i/m_s$$

where $\underline{q}_i$ and $\underline{p}_i$ are the positions and momenta of the ith atom; m_s is the mass of a surface atom and the brackets indicate spatial averaging over the wavefunction

$$\langle f \rangle \equiv \int_{-\infty}^{+\infty} \Psi^* (\underline{R})\, f\, (\underline{R})\, \Psi(\underline{R})\, d\underline{R} \,. \qquad (2.4)$$

The consistency of the integration scheme is checked by turning off the bulk interactions in Equations (2.2) and (2.3). The averaged Hamiltonian becomes a constant of the motion

$$\frac{d}{dt} \langle H \rangle = 0 \qquad (2.5)$$

where $\langle H \rangle$ is the mixed quantum-classical energy defined by

$$\langle H \rangle = \sum_{i=1}^{4} \frac{p_i^2}{2m_s} + V_{surf} + \langle V(\underline{R},\underline{r}(t)) \rangle + \left\langle -\frac{\nabla^2}{2m} \right\rangle \qquad (2.6)$$

The integration scheme described by Equations (2.2) to (2.5) is a general, consistent treatment of a mixed classical-quantum calculation.

To include the dynamics of the bulk atoms, a reduction scheme is needed in which only the part of the motion influencing the He and the surface atoms is relevant and need be treated explicitly. For the

He-bulk interaction only the static contribution is included in the calculation. This form is chosen to incorporate a physically reasonable asymptotic form.[19] For the surface atoms the bulk behaves as a heat bath. In this work the bulk dynamics is simulated by a Generalized Langevin Equation (GLE) description adapted from the work of Adelman and Doll.[7-9] The bulk is represented by a chain of coupled ghost atoms in which the last atom in the chain is subject to a random force and friction. The friction and random force are balanced by the fluctuation-dissipation theorem to maintain the chain at the correct temperature. This chain can be constructed in such a way that the correct response function of the bulk is matched. Following Tully,[11] these coupled equations are written as

$$\begin{aligned} \ddot{\underline{r}}(t) &= -\Omega_p^2\, \underline{r}(t) + \Lambda_o^{1/2}\, \omega_o \underline{s}(t) + \underline{F}_p[\underline{r}(t), \underline{s}(t), z_o] \\ \ddot{\underline{s}}(t) &= \Lambda_o^{1/2}\, \omega_o \underline{r}(t) - \omega_o^2 \underline{s}(t) - \gamma\, \underline{s}(t) + \underline{\xi}(t) \end{aligned} \tag{2.7}$$

where $\underline{s}$ is the vector describing the ghost atoms which are harmonically coupled with the primary cell atoms by a frequency $\Lambda_o^{1/2}\omega_o$ and individually by ω_o^2. Ω_p^2 is the primary cell harmonic response and $\underline{F}_p$ is the cell-ghost force. The frictional constant γ and Gaussian random function $\underline{\xi}(t)$ are related by

$$\langle \underline{\xi}(o)\underline{\xi}^{+}(t) \rangle = 2kT\gamma\delta(t) \tag{2.8}$$

These equations fulfill the conditions demanded by the second fluctuation-dissipation theorem.

B. Computational Background

The quantum mechanical description of the colliding He atom is given by a time dependent solution of the Schrödinger equation with a time dependent potential. The integration method used is the Fourier method given in detail previously.[15-16] In the Fourier method the wavefunction is represented on a spatial grid The potential energy operator is diagonal in this representation, so that the operation $V*\Psi$ is a simple multiplication. The kinetic energy operator, $-\nabla^2/2m_s$ is calculated by transforming Ψ to the diagonal P reprsentation with a discrete Fourier transform, multiplying by $P^2/2m_s$ and transforming back to R space by an inverse discrete Fourier transform. The time propagation is achieved by second order differencing which preserves the norm and energy of the particle as well as the time reversed symmetry of the Schrödinger equation. The main advantages of the method are high accuracy in representing the kinetic energy operator and numerical efficiency due to the Fast Fourier Transform (FFT) algorithm.[19]

Because the method has been described previously[15-16] only those alterations required for surface scattering are described here. The first step is to define the spatial region to be represented and to discretize it by a proper choice of grid The interval between grid points is determined by calculating the maximum momentum, P_{max}, which can occur in each spatial direction so that the grid size is given by

$$\Delta x = \pi/P_{max} \qquad (2.9)$$

The Fourier method, because it involves the discretization of a Fourier transform, necessarily uses periodic boundary conditions. In the spatial directions parallel to the surface the periodic boundary conditions are matched to the unit cell. In the normal direction to the surface the periodic conditions introduce an unphysical constraint on the propagating wavefunction. This drawback is partially alleviated by the repulsive part of the surface potential which prevents the wavefunction from "wrapping around" the interval when approaching the surface. On the other end, however, the wavefunction must be matched to a freely propagating solution. The periodic boundary conditions imply that the wave is reflected from the back side of the repulsive part of the surface potential when the end of the grid is reached. A solution to this difficulty was found by applying absorbing boundary conditions on the free side. Earlier attempts to use an optical (imaginary) potential failed because the resulting Hamiltonian was not Hermitian and the stability properties of the Fourier method were lost.

The solution proposed here entails construction of a buffer zone at the end of the grid with a width of 8-20 points. In this zone the wavefunction is absorbed gradually in order to eliminate reflections. The absorption is achieved by multiplying the wavefunction in the zone by a decreasing sequence after each time step. The sequence used was $\exp[-g(n-n_o)^2]$ where n_o is the grid position of the absorbing boundary; n is a grid position within the zone and g is an adjustable parameter. Numerical tests performed with a wavefunction moving toward the boundary showed a residual reflection of 10^{-3} using an absorbing

zone of 14 points. The parameter g and the width of the buffer zone must be chosen according to the average momentum of the approaching wavefunction. If the absorption is too fast reflections appear at the boundary; if it is too slow reflections occur at the end of the grid.

The details of the bulk and surface interactions are taken from the work of Shugard, Tully and Nitzan [10] for one dimensional desorption and from Tully[11] and Grimmelmann, Tully and Helfand[12] for the three dimensional simulation. In the combined description of the quantum and classical motion, the accuracy of the quantum integration determines the time step. The classical integration is done with a Runge-Kutta-Gill procedure using this same time step. At each cycle in the integration the positons of the primary atoms are transferred to the quantum integrator where the interaction potential is calculated and the wavefunction advanced one time step. The average forces are then calculated and fed back to the classical motion. A check on the accuracy of this scheme was performed by turning off the bulk interaction and evaluating the mixed quantum-classical energy. The error was of the order 10^{-6} using single precision on a VAX 750/11.

III. Desorption of He from a Tungsten Surface

As a first application of this technique, one dimensional desorption of helium atoms from tungsten was simulated. A typical run was started by centering a Gaussian wave packet on the attractive wall of the atom-surface potential. The interaction potential was chosen to be a Morse interaction of the form

$$V_{\text{He-surf}}(r,R) = D\left[e^{-2\alpha(r-r_c)} e^{-2\alpha R} - 2\, e^{-\alpha(r-r_c)} e^{-\alpha R}\right] \qquad (3.1)$$

where D = .0012 a.u., α = 1.2 bohr^{-1} and r_c = 2.0 bohr. The initial total energy was negative, insuring that the He is initially bound to the surface. Equations (2.2) and (2.7) were then propagated in time. The bulk and coupling parameters were chosen in accordance with the Debye model[9]

$$\omega_D = 1.04 \times 10^{-3}$$

$$\Omega_p^2 = 3/5\ \omega_D^2$$

$$\Lambda_o^{1/2}\omega_o = (12/175)^{1/2}\omega_D^2$$

$$\omega_o^2 = \omega_D^2/3$$

$$\Upsilon = \pi\omega_D/6$$

A Gaussian random force is chosen for $\xi(t)$ which is balanced by friction on the secondary atoms in such a way as to preserve the temperature of the system. The standard deviation for this distribution is determined by the temperature of the solid, $\sigma^2 = (6kT\Upsilon/m_s)$. A grid of 128 points was used with a spatial step size Δx = .2 bohr. The last 14 points on the grid were used for the absorbing boundary terms discussed above. A time step of .2 atomic units was found to be sufficiently accurate and stable.

A typical desorption simulation displays all the physical effects expected of a realistic model. The thermal motion of the surface atoms transfers energy to and from the He atom allowing it to dissociate

from the surface. As time progresses, the probability that the initial wavepacket leaves the surface is monitored Figure 1 displays a sequence of snapshots of the evolving wavefunction superimposed on the dynamic atom-surface potential. For comparison, the wavepacket distribution on momentum space is also shown above the position space wavefunction. The last figure shows the absorption of the wavepacket by the boundary terms. The rate of desorption is determined by examining the normalization of the wavepacket as a function of time. Figure 2 presents a typical plot of the logarithm of the normalization versus time. After an initial lapse time, the decay becomes approximately exponential with superimposed fluctuations caused by the random character of the classical motion. The average slope of this graph is the desorption rate. An improved decay probability was obtained by averaging over the initial conditions for the simulation. The number of runs used for the averaging varied from 1 to 4 as the temperature was lowered The results do not depend sensitively upon the averaging procedure Figure 3 displays these results for several different temperatures An examination of Figure 3 suggests that the desorption mechanism changes at higher temperatures - above approximately 300 K. A possible explanation for this behavior is that at low temperatures the desorption proceeds by a ladder mechanism with the He atom gradually acquiring more energy until it dissociates. At higher temperatures, a direct or one-step mechanism applies.

IV. Scattering of He from Pt - A Three Dimensional Simulation

A quantum mechanical three dimensional calculation of scattering from a dynamical surface is a computational challenge. This challenge is worth taking because such a calculation realistically describes a

scattering or desorption experiment. One of the more difficult steps in the calculation entails quantum mechanical propagation of the scattering particle. In this section, the one dimensional analysis above is extended to scattering in three dimensions while retaining the classical description of the dynamical surface.

The unit cell of the metal defines the extent of the surface in which to continue the He atom. The static contribution to the potential energy, following Grimmelmann et al.[12], is chosen to be

$$v(z) = D_z \left[\frac{2}{15}\left(\frac{a_z}{z+z_o}\right)^9 - \left(\frac{a_z}{z+z_o}\right)^3\right] \tag{4.1}$$

with parameter values D_z = 2 meV, a_z = 4.62 Å and z_o = 0.904 Å. The dynamical potential is constructed from a pairwise 6-12 Lennard-Jones interaction between the He atom and each of the Pt atoms

$$V_{dyn}(t) = D_o \sum_{i=1}^{4} \left[\left(\frac{R_o}{R_i(t)}\right)^{12} - \left(\frac{R_o}{R_i(t)}\right)^{6}\right], \tag{4.2}$$

where $R_i(t)$ is the time dependent magnitude of the distance between the He atom and the ith Pt atom in the unit cell, D_o = 3 meV, and R_o = 3.80 Å. Another contribution to the static potential arises from the twelve Pt atoms adjoining the unit cell. These contributions are also assumed to be represented by the Lennard-Jones form of Eqn. (4.2) but

without the time dependence. The total static contribution is thus

$$V_{static} = V(t) + D_o \sum_{j=1}^{12} \left[\left(\frac{R_o}{R_j}\right)^{12} - \left(\frac{R_o}{R_j}\right)^{6}\right] \tag{4.3}$$

Periodic boundary conditions are used to simulate the extended part of the surface.

To perform the scattering calculation accurately, it is necessary to choose the edge of the grid, in the perpendicular z-direction, to be in the asymptotic region of the surface potential. The number of grid points is again determined by the maximum momentum which must be represented in each degree of freedom, as in Eqn. (2.9). In the present case, the maximum momentum is estimated by the relation

$$P_{max} = \sqrt{2m(E-V_{min})} \tag{4.4}$$

For the specific case of He scattering from Pt, an adequate grid for the (x,y,z) directions is given by (16,16,64) points since the well depth is 1.8×10^{-4} Hartrees (4.9 meV) and the unit cell size is 3.81 Å. The grid size essentially determines the accuracy of the calculation and is the major computational restriction in terms of memory required. A (16,16,64) grid was approximately 1.24×10^{5} words of memory. By comparison, a finite difference scheme would require 125 times more words to achieve comparable accuracy.

The propagation of the wavefunction was performed by using the simple differencing scheme

$$\Psi_{n+1} = \Psi_{n-1} - (2i\ dt)\ H\Psi_n \tag{4.5}$$

The kinetic energy contribution in HΨ was calculated by using a three dimensional FFT routine while the static potential energy part is simply a multiplication. The twelve coordinates of the four surface atoms in the unit cell were used to calculate the dynamical part of VΨ and this term is added to the static contribution. The twelve averaged forces necessary for the classical integrator are also calculated at each time step and returned to the classical mechanical equations of motion. The Langevin parameters for the surface motion, described by the system of equations in (2.7) were taken from Tully.[11] The resulting 48 coupled ordinary differential equations were integrated by a Runge-Kutta Gill procedure. To determine the relative computational effort induced by the dynamical potential, a completely static surface potential run was performed. There is, approximately, a 50% increase in computational time due chiefly to the calculation of the dynamical potential at each step. For comparison purposes, timing runs were made on different computers. A single precision time step used 80 seconds in a VAX 750/11 with a UNIX operating system; 36 seconds on a VAX 780; 6 seconds on an FPS-164 array processor; and 1.4 seconds on a CRAY-1.

The actual scattering event was simulated by placing the initial Gaussian wave packet in the asymptotic region of the surface potential with a non-zero z-momentum component. The parameters chosen for this simulation are summarized in Table 1. Two extreme temperatures, 100 K and 800 K, were chosen for comparison, keeping all other parameters fixed. Figures 4 and 5 depict the scattering event in configuration space as a function of time for 100 K and 800 K respectively. Figures 6

and 7 show the same collision in the momentum representation. As may be seen from the figures, there is significant non-specular scatter. The main effect of the surface motion is to broaden the wave packet after collision; an effect which is more pronounced at the higher temperature.

The calculations above represent a first step toward a realistic description of time dependent particle-surface scattering phenomena. A classical description of the surface is adequate for the light particle-massive surface scattering over a large temperature range. The difficult quantum propagation of the scattering particle is accurately handled by the Fourier transform technique The present results demonstrate the feasibility of this computational scheme. Currently, this technique is being used to study three dimensional desorption phenomena to assess the effect of more spatial dimensions upon the change in the desorption mechanism observed in the one dimensional case. Also, the importance of the dynamical motion of the atoms adjoining the unit cell is being studied. The technique presented here appears to be quite versatile and offers a viable approach to describing particle-surface interactions.

Acknowledgements

The authors are grateful to Profs. S. A Rice and J. C. Light for their encouragement and for allowing the use of the computational facilities and resources of the James Franck Institute where part of this work was performed. This work has been performed under the auspices of the U. S. Department of Energy by the Lawrence Livermore National Laboratory under Contract No. W-7405-ENG-48.

References

1. T. Engel and K. H. Rieder in Structural Studies of Surfaces, G. Hohler, ed., Springer Tracts in Modern Physics 91, Springer-Verlag (Berlin), 1982.

2. R. B. Doak, U. Harten and P. Toennies, Phys. Rev. Lett. 51, 578(1983); K. C. Janda, J. E. Hurst, C. A. Becker, J. P. Cowin, D. J. Auerbach and L. Wharton, J. Chem. Phys. 72, 2403 (1980).

3. M. Sinvani, M. W. Cole, and D. L. Goodstein, Phys. Rev. Lett., 51, 188 (1983).

4. G. Wolken, J. Chem. Phys. 58, 3047 (1973); H. Chow and E. D. Thompson, Surf. Sci. 59, 225 (1976).

5. J. W. Hutson and C. Schwartz, J. Chem. Phys. 79, 5179 (1983); R. B. Laughlin, Phys. Rev. B25, 2222 (1982); N. Garcia, V. Celli, and F. O. Goodman, Phys. Rev. B19. 20 (1979).

6. J. D. Doll, Chem. Phys. 3, 257 (1974).

7. S. A. Adelman and J. D. Poll, J. Chem. Phys. 61, 4242 (1974).

8. S. A. Adelman and J. D. Doll, J. Chem. Phys. 64, 3375 (1976).

9. S. A. Adelman in Advances in Chemical Physics, Vol. XLIV, I. Prigogine and S. A. Rice eds., Wiley-Interscience (New York) 1980.

10. M. Shugard, J. C. Tully, and A. Nitzan, J. Chem. Phys. 66, 2534 (1977).

11. J. C. Tully, J. Chem. Phys. 73, 1975 (1975).

12. E. K. Grimmelmann, J. C. Tully, and E. Helfand, J. Chem. Phys. 74, 5300 (1981).

13. E. A. McCullough and R. E. Wyatt, J Chem. Phys. 51, 1253 (1969); E. A. McCullough and R. E. Wyatt, J. Chem. Phys. 54, 3578 (1971); K. C. Kulander, J. Chem. Phys. 69, 5064 (1978); A. Askar and S. Cakmak, J. Chem. Phys. 36, 2794 (1978).

14. P. M. Agrawal and L. M. Raff, J. Chem. Phys. 77, 3946 (1982).

15. D. Kosloff and R. Kosloff, J. Comp. Phys. 52, 35 (1983).

16. R. Kosloff and D. Kosloff, J. Chem. Phys. 79, 1823 (1983).

17. G. Drolshagen and E. J. Heller, J. Chem. Phys. 79, 2072 (1983).

18. A. T. Yinon and R. Kosloff, Chem. Phys Lett. 102, 216 (1983).

19. H. J. Nussbaumer, Fast Fourier Transforms and Convolution Algorithms, 2nd edition, Springer-Verlag (Berlin) 1982.

Table 1

Parameters used in three dimensional scattering of He from Pt bcc (100)

(atomic units)

Integration Grid		Wavepacket Initial Conditions			Surface/Bulk Parameters
time	increment	5.0	z_o	16.5	$m_s = 3.555 \times 10^5$
x	increment	0.45	k_x	0.0	$\Omega_d = 7.44 \times 10^{-4}$
y	increment	0.45	k_y	3.0	$\Omega_g = .5032\ \Omega_d$
z	increment	0.40	k_z	-2.9	$\beta = 0.5236\ \Omega_d$
total time steps		12×10^3	σ_z (width)	3.3	$r_o = \left(\frac{3kT}{m_s}\right)^{1/2}$
					$\sigma = \left(\frac{6kT\beta}{m_s}\right)^{1/2}$

Figure Captions

Figure 1. (a) - (d) One dimensional desorption of a helium wavepacket as a function of time at 800 K. The dynamic surface potential is superimposed upon the coordinate space representation (lower graph). The upper graph displays the momentum space representation of the wavepacket.

Figure 2. Representative plot of the logarithm of the one dimensional wavepacket normalization as a function of time.

Figure 3. Inverse temperature plot of the logarithm of the one dimensional averaged desorption rates.

Figure 4. (a) - (e) Three dimensional scattering of He from Pt at 100 K in coordinate space. The amplitude of the wavepacket is plotted in the z-x plane with the solid surface at the left edge of the graph.

Figure 5. (a) - (e) Same as Figure 4 at 800 K.

Figure 6. (a) - (e) Momentum space representation of the wavepacket amplitude in Figure 4. Several k_x values are fixed for all values of k_y and k_z at 100 K.

Figure 7. (a) - (e) Same as Figure 6 at 800 K.

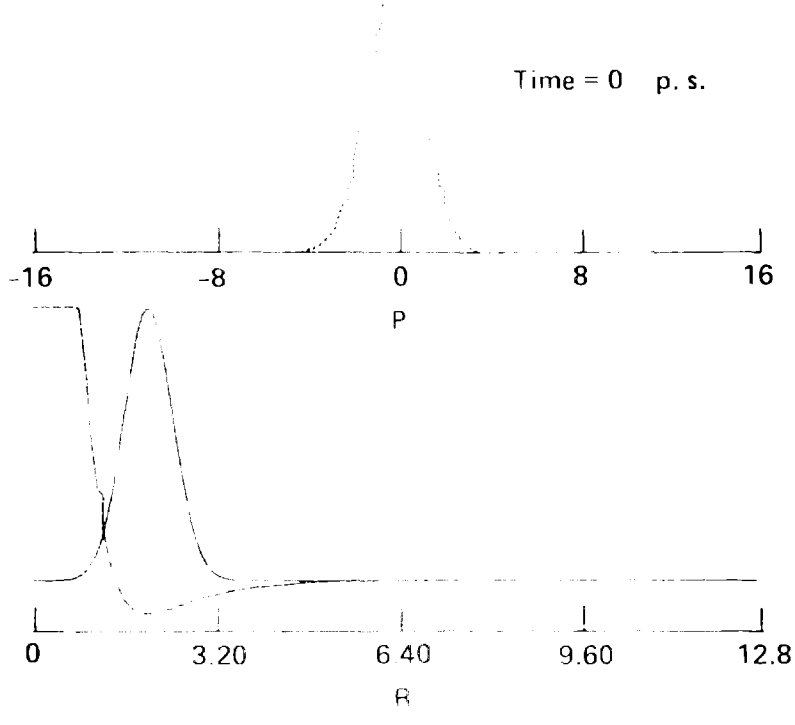

Fig 16(a)
Caption

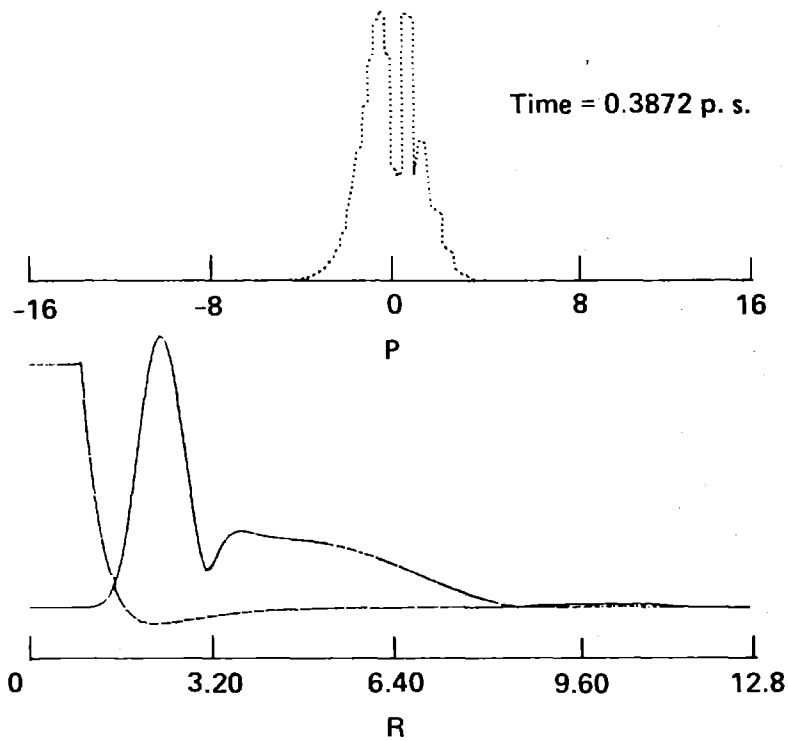

Fig 4.(b)
Contin

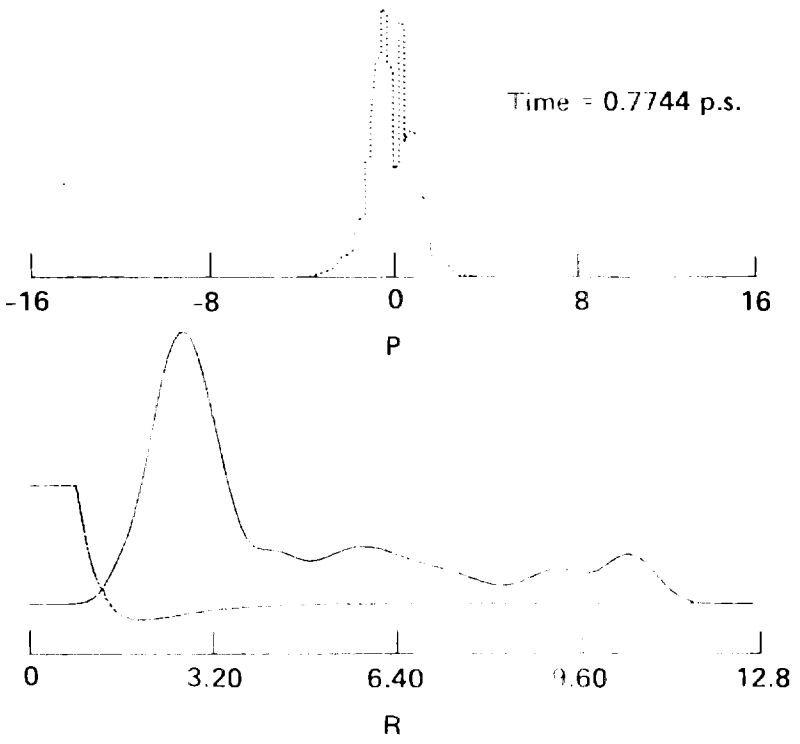

Fig 1(c)

Cerium

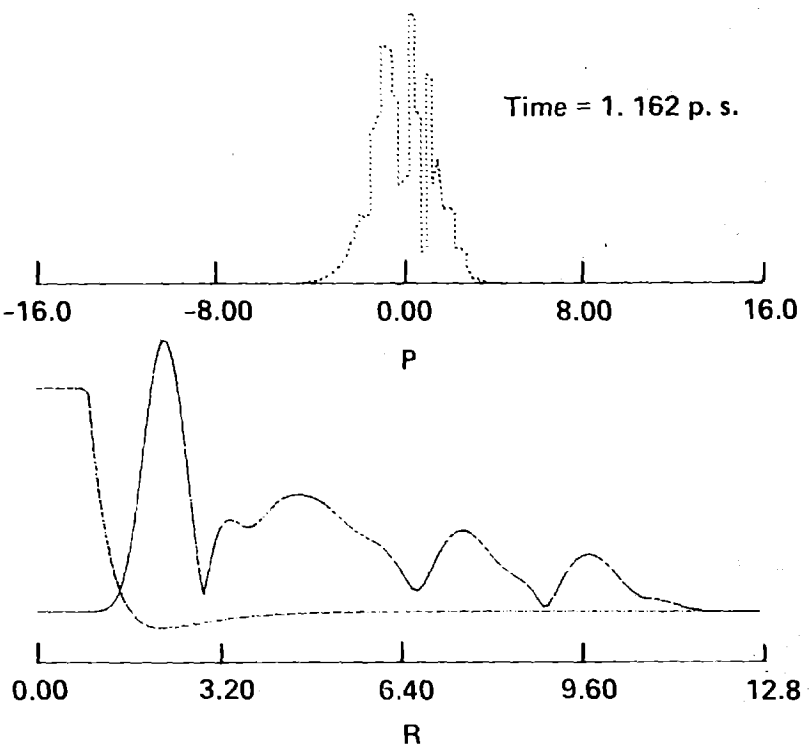

Fig 1(d)

Cerjan

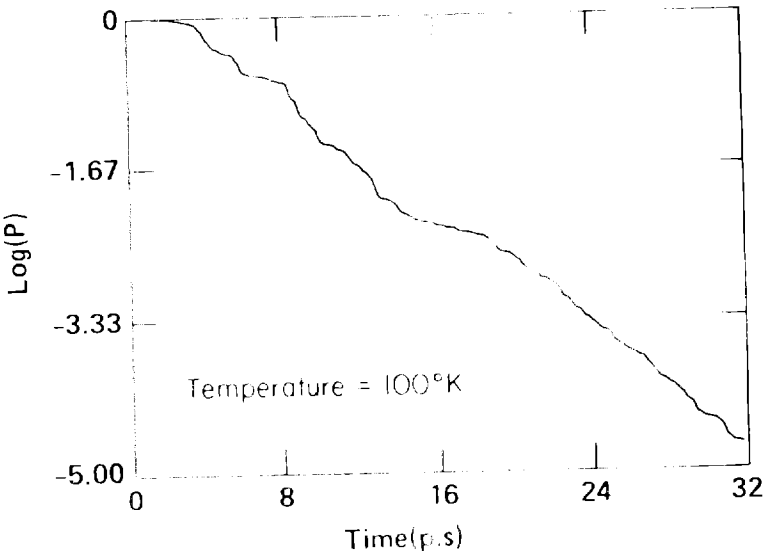

Fig. 2

Cerjan

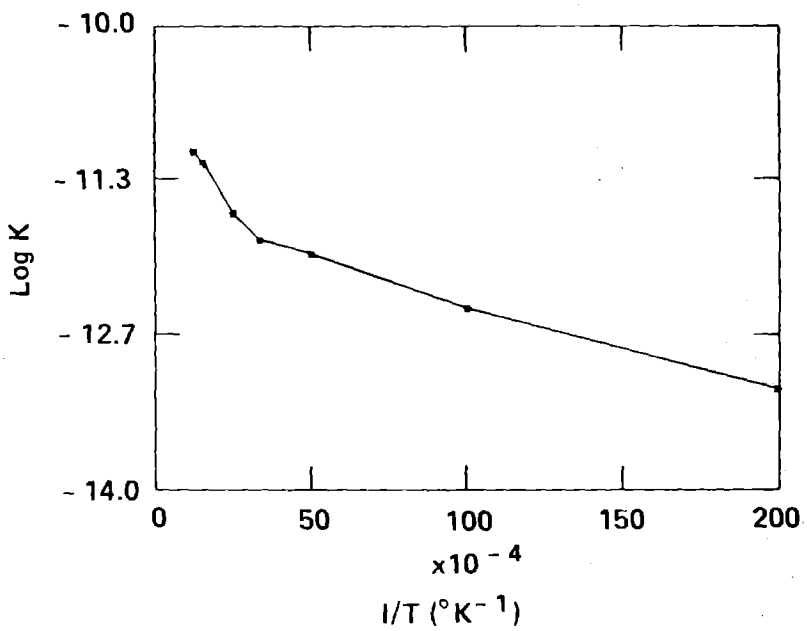

Fig 3

Cerjan

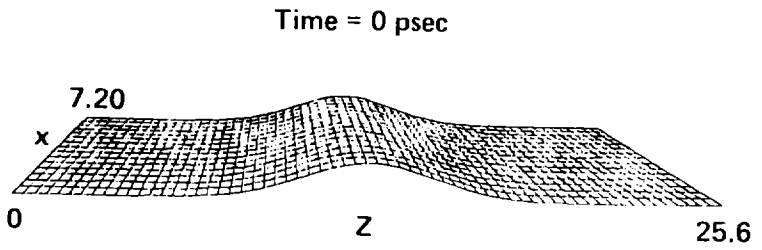

Fig 4 (a)

Cerjan

Time = 0.64 psec

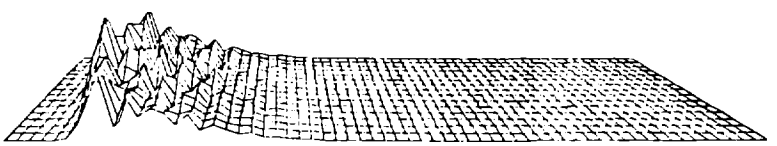

Fig 4(b)

Cerjan

Time = 0.82 psec

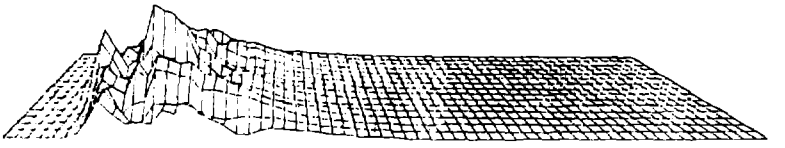

Fig 4(c)

Cerjan

Time = 0.99 psec

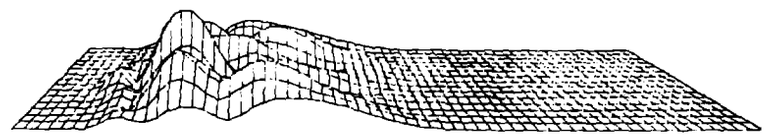

Fig 4(a)

Cerjan

Time = 1.36 psec

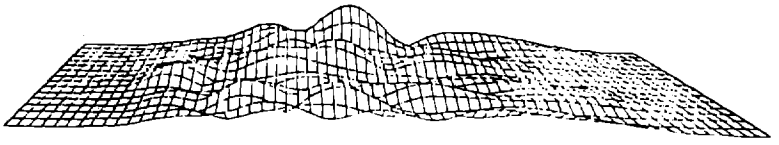

Fig 4(e)

Cerjan

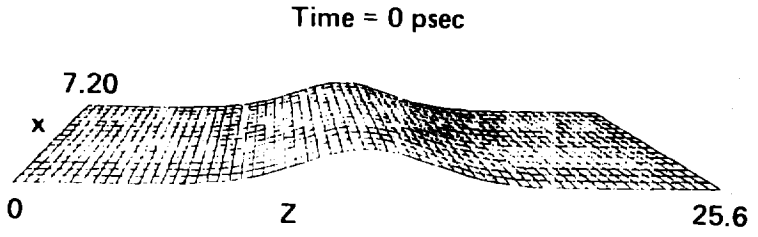

Fig 5(a)

Cerjak

Time = 0.64 psec

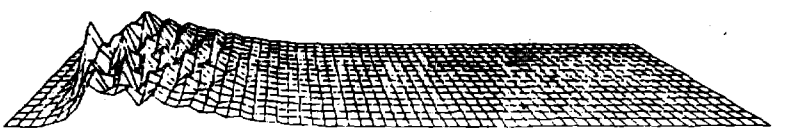

Fig 5(b)

Cerjan

Time = 0.82 psec

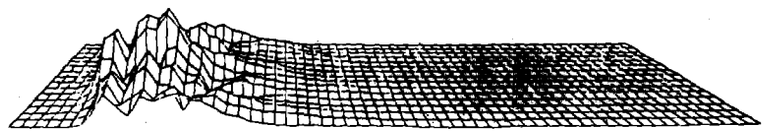

Fig 5(c)

Cerjan

Time = 0.99 psec

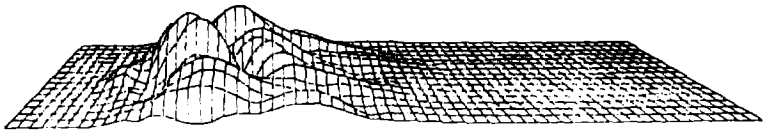

Fig 5(d)

Cerjan

Time = 1.36 psec

Fig 5(c)

Carjan

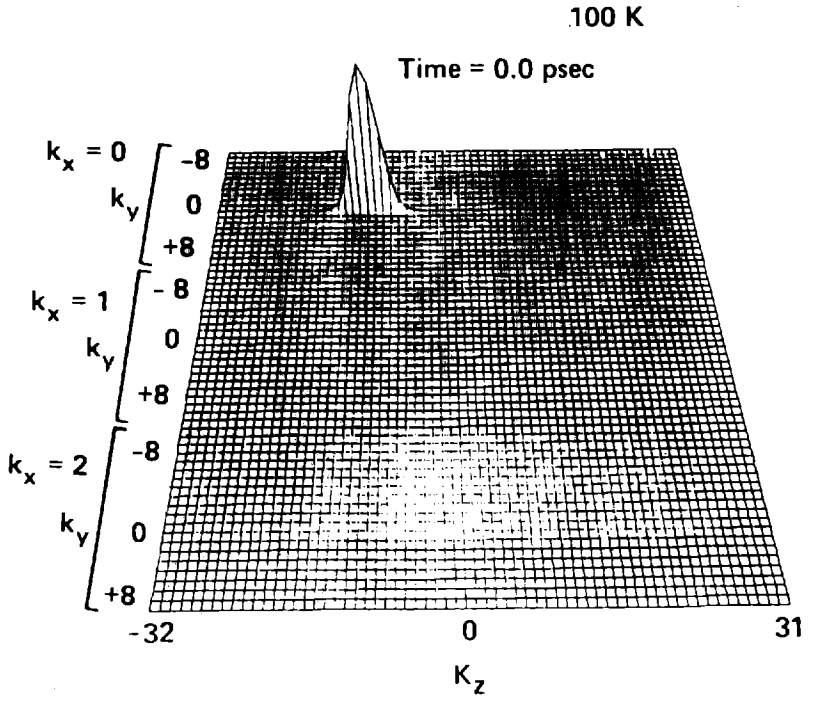

Fig 6(a)

cerjak

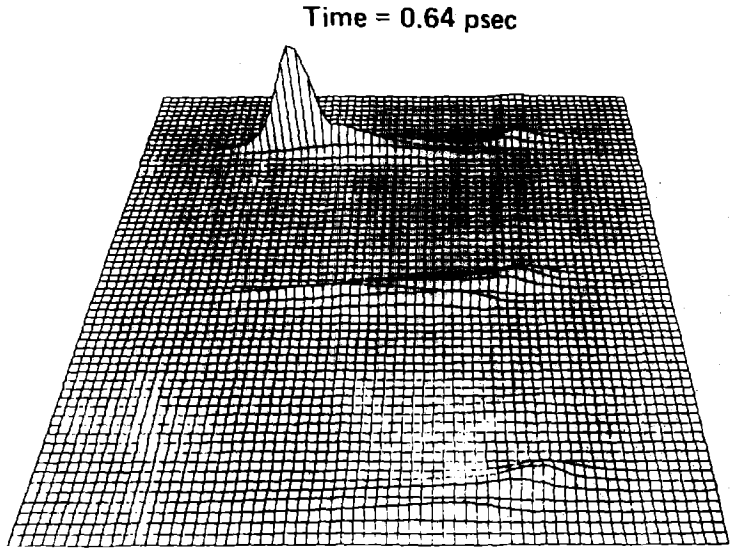

Fig 6(b)

Cerjan

Time = 0.82 psec

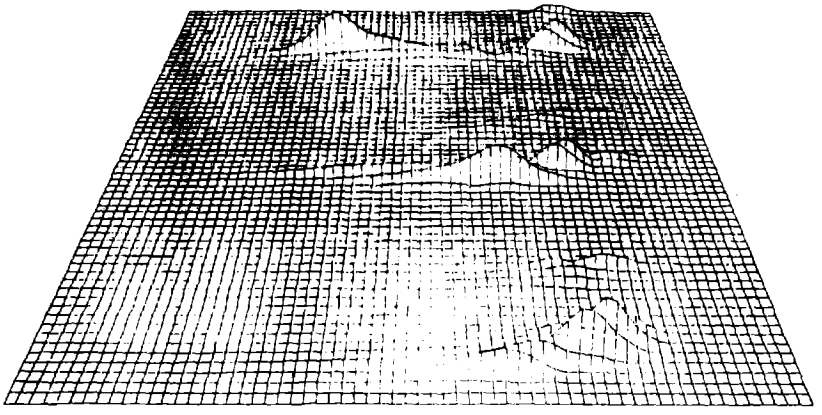

Fig 6(c)

Ceram

Time = 0.99 psec

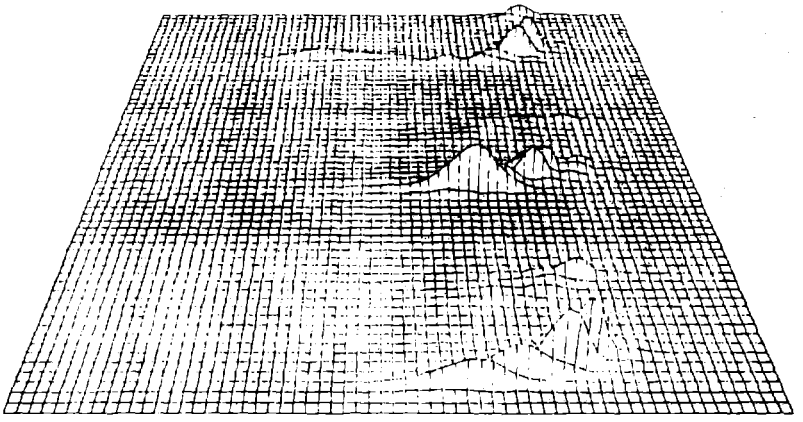

Fig 6(d)

Cerjan

Time = 1.36 psec

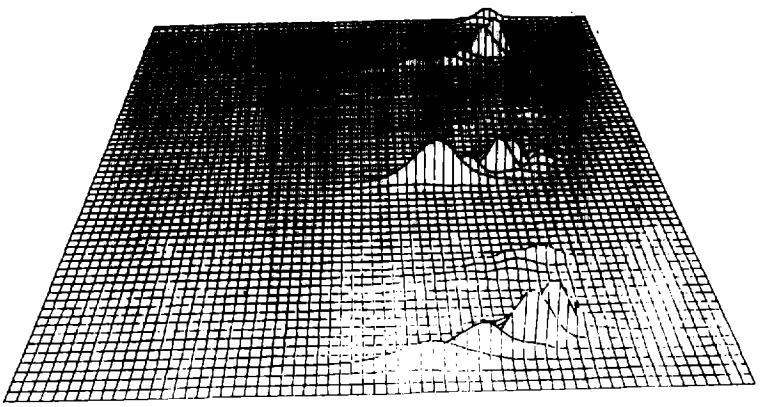

Fig 6(c)

Carjan

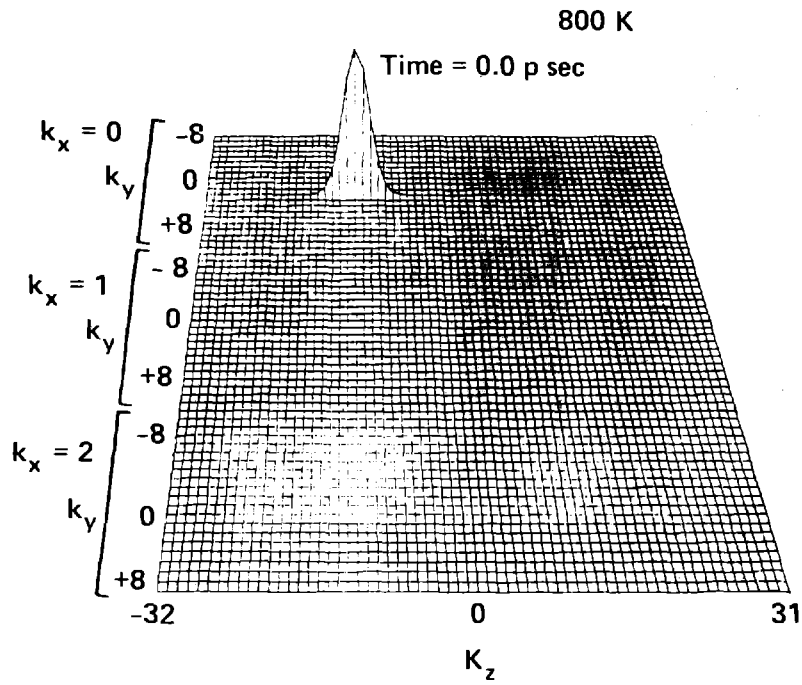

Fig 7(a)
Cerjan

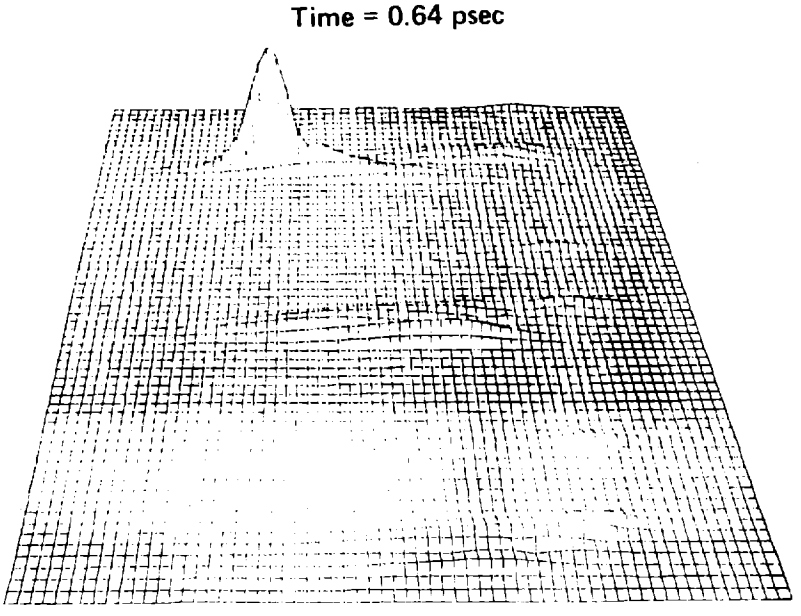

Fig 7(b)

Corjkn

Time = 0.82 psec

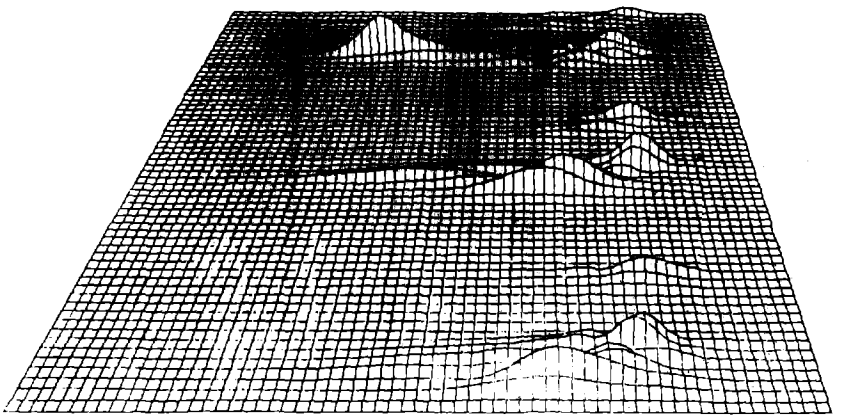

Fig 7(c)

Cerjan

Time = 0.99 psec

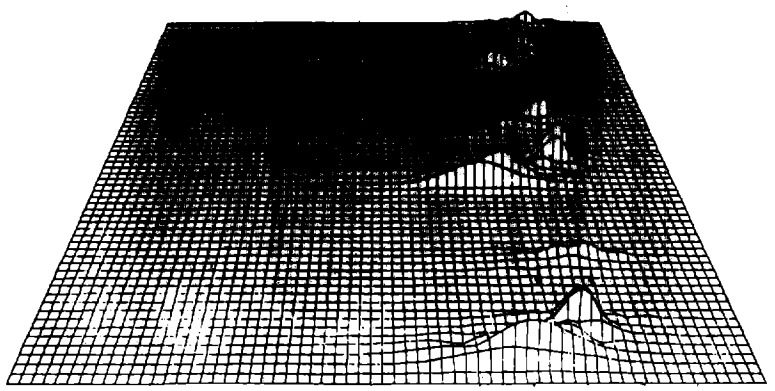

Fig 7(d)

Carjan

Time = 1.36 psec

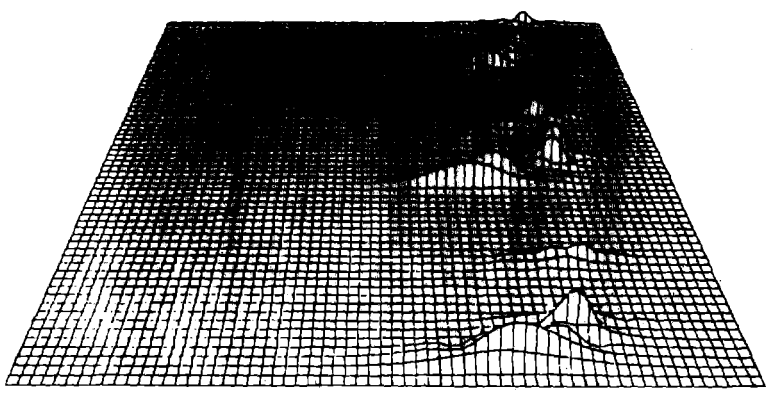

Fig 7(e)